

FULL PAPER

Open Access



# Pre-eruption magmatic processes and magma plumbing system at Hachijo-Nishiyama volcano, Izu–Bonin arc, Japan

Kazuki Oiwa<sup>1,2</sup>, Takeshi Kuritani<sup>3\*</sup> , Mitsuhiro Nakagawa<sup>3</sup> and Shumpei Yoshimura<sup>3</sup>

## Abstract

Nishiyama volcano on Hachijojima Island is an active basaltic volcano located in the Izu–Bonin arc. In this study, petrological and geochemical analyses were conducted on mafic lavas and pyroclastics to understand the magma plumbing system and pre-eruption magmatic processes. Whole-rock major element compositions show significant variations (49.4–54.9 wt.% SiO<sub>2</sub>), and the samples contain variable amounts of plagioclase phenocrysts (1–40 vol.%). The whole-rock Sr, Nd, and Pb isotopic compositions of samples from the youngest volcanic stage (< 0.7 ka) are homogeneous, whereas some samples from the older stage (3–1 ka) have relatively low Pb isotopic ratios. This observation suggests that the younger magmas were derived from a single parental magma, but another parental magma with distinct geochemical features was involved in the magmatic system before 1 ka. The temporal variation in the FeO\*/MgO ratios of the volcanic products is complex and is considered to reflect the intermittent injection of primitive magmas into the main magma chamber in which fractional crystallization occurred. Two-pyroxene geobarometry suggests that the main magma chamber was located at a depth of 9–12 km. The core region of some plagioclase phenocrysts consists of a glass inclusion-free inner core and an inclusion-rich outer mantle, suggesting that some plagioclase crystallized in the main magma chamber, which was followed by overgrowth during magma ascent because of increasing liquidus temperatures due to decompression-induced water exsolution from the melt. The whole-rock compositions of some eruption units with different Al<sub>2</sub>O<sub>3</sub>/MgO ratios exhibit distinct plagioclase-controlled trends, which negates the possibility that plagioclase accumulation occurred in a stable magma chamber. In addition, the density of plagioclase was higher than that of the melt during the magma ascent to the surface. From these observations, it is suggested that the accumulation of plagioclase phenocrysts occurred in ascending magmas as the plagioclase settled relative to the surrounding melt. The estimated depth of 9–12 km for the main magma chamber coincides with the depth range over which earthquake swarms occurred in 2002, suggesting that the magma chamber is still active, and that the earthquake swarms may reflect the injection of primitive magma into the magma chamber.

**Keywords** Active volcano, Magma plumbing system, Magmatic differentiation, Plagioclase accumulation, Water content

\*Correspondence:

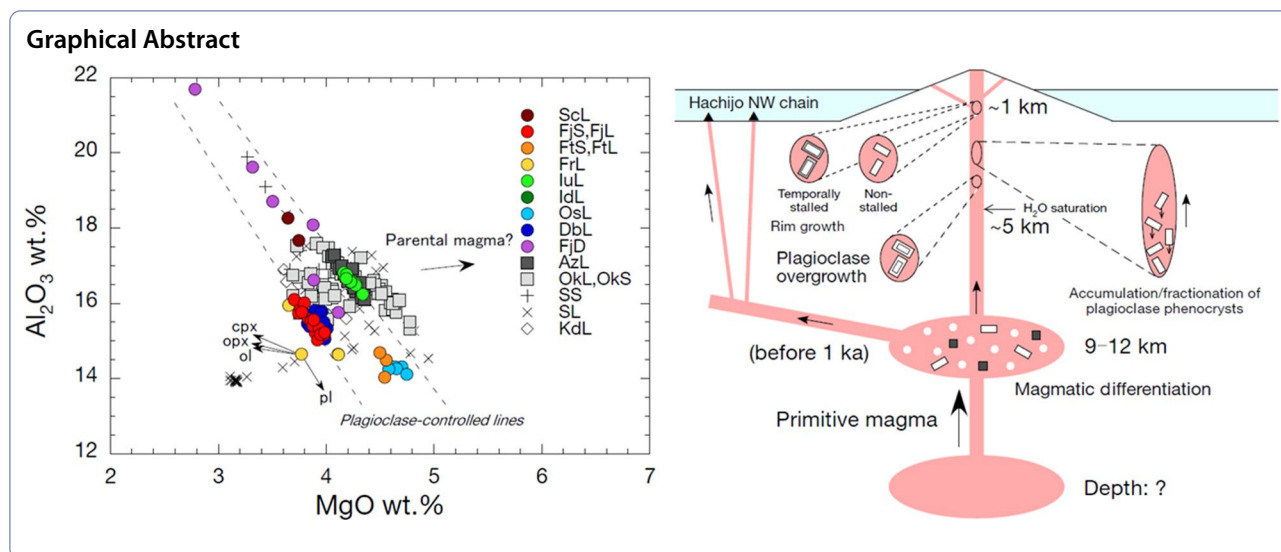
Takeshi Kuritani

kuritani@sci.hokudai.ac.jp

Full list of author information is available at the end of the article



© The Author(s) 2023. **Open Access** This article is licensed under a Creative Commons Attribution 4.0 International License, which permits use, sharing, adaptation, distribution and reproduction in any medium or format, as long as you give appropriate credit to the original author(s) and the source, provide a link to the Creative Commons licence, and indicate if changes were made. The images or other third party material in this article are included in the article's Creative Commons licence, unless indicated otherwise in a credit line to the material. If material is not included in the article's Creative Commons licence and your intended use is not permitted by statutory regulation or exceeds the permitted use, you will need to obtain permission directly from the copyright holder. To view a copy of this licence, visit <http://creativecommons.org/licenses/by/4.0/>.



### Introduction

Hachijojima is an active volcanic island located on the volcanic front of the Izu–Bonin arc (Fig. 1a). The north-western part of the island is mainly made up of basaltic products of younger volcanism (<~10 ka) that constitute Nishiyama volcano (Fig. 1b). Although magmatic eruptions have not occurred for more than 400 years since the latest eruption in 1605 AD, the magmatic system remains active, as suggested by the earthquake swarm activities in 2002 AD (Ishizuka and Geshi 2018). To understand the recent magma plumbing system and/or magmatic processes at Hachijojima, petrological and geochemical studies have been conducted on volcanic products from the Nishiyama volcano (Isshiki 1958, 1963; Nakano et al. 1991, 1997; Tsukui and Hoshino 2002; Ishizuka et al. 2008; Aizawa et al. 2020).

Nakano et al. (1991) showed that whole-rock  $Al_2O_3$  contents of basaltic products from the Nishiyama volcano correlate positively with the abundance of plagioclase phenocrysts, suggesting that the whole-rock compositional variation is primarily controlled by plagioclase fractionation or accumulation ('plagioclase control'). Tsukui and Hoshino (2002) divided the Nishiyama volcanic products into three groups based on whole-rock compositions and the abundance of plagioclase phenocrysts, and showed that the intra- and inter-group compositional variations can be explained by crystal

fractionation or accumulation and magma mixing. Ishizuka et al. (2008) examined whole-rock compositional variations of the products of the Nishiyama volcano, as well as those of submarine volcanic products surrounding Nishiyama ("Hachijo NW chain", "Hachijo-kojima chain", and "NE edifices" in Fig. 1b), and found that some submarine samples have primitive compositions. They suggested that the magma plumbing system consisted of a deep magma chamber (>20 km depth), a middle magma chamber (10–20 km depth), and a shallow magma chamber (<5 km), and that crystal fractionation or accumulation occurred in the shallow magma chamber. Aizawa et al. (2020) conducted a petrological study on anorthosite enclaves in lavas from the Nishiyama volcano. They suggested that the enclaves were produced in the shallow magma chamber under  $H_2O$ -saturated conditions and that they represent accumulated plagioclase crystals that were involved in the formation of the plagioclase-controlled whole-rock compositional variation.

Recently, Ishizuka and Geshi (2018) presented a detailed geological map of Hachijojima Island, which enabled us to collect samples with good temporal resolution from the Nishiyama volcano. Using this new information, we conducted petrological and geochemical analyses of subaerial eruptive products from the Nishiyama volcano to understand the magma plumbing system and pre-eruption magmatic processes, particularly those

(See figure on next page.)

**Fig. 1** **a** Map showing the locality of Hachijojima Island and **b** topographical map. In **a**, triangles indicate the locations of active volcanoes. The slab depths were sourced from Kita et al. (2010) and Liu and Zhao (2016). The solid and dashed contour lines denote the depths of the upper boundaries of the subducting Pacific and Philippine Sea slabs, respectively (Liu and Zhao 2016). The blue lines denote the plate boundaries at the surface. In **b**, the localities of submarine "Hachijo NW chain", "Hachijo-kojima chain", and "NE edifices", consisting of many satellite cones (small triangles) and chains of vents (bars), are also shown (Ishizuka et al. 2008)

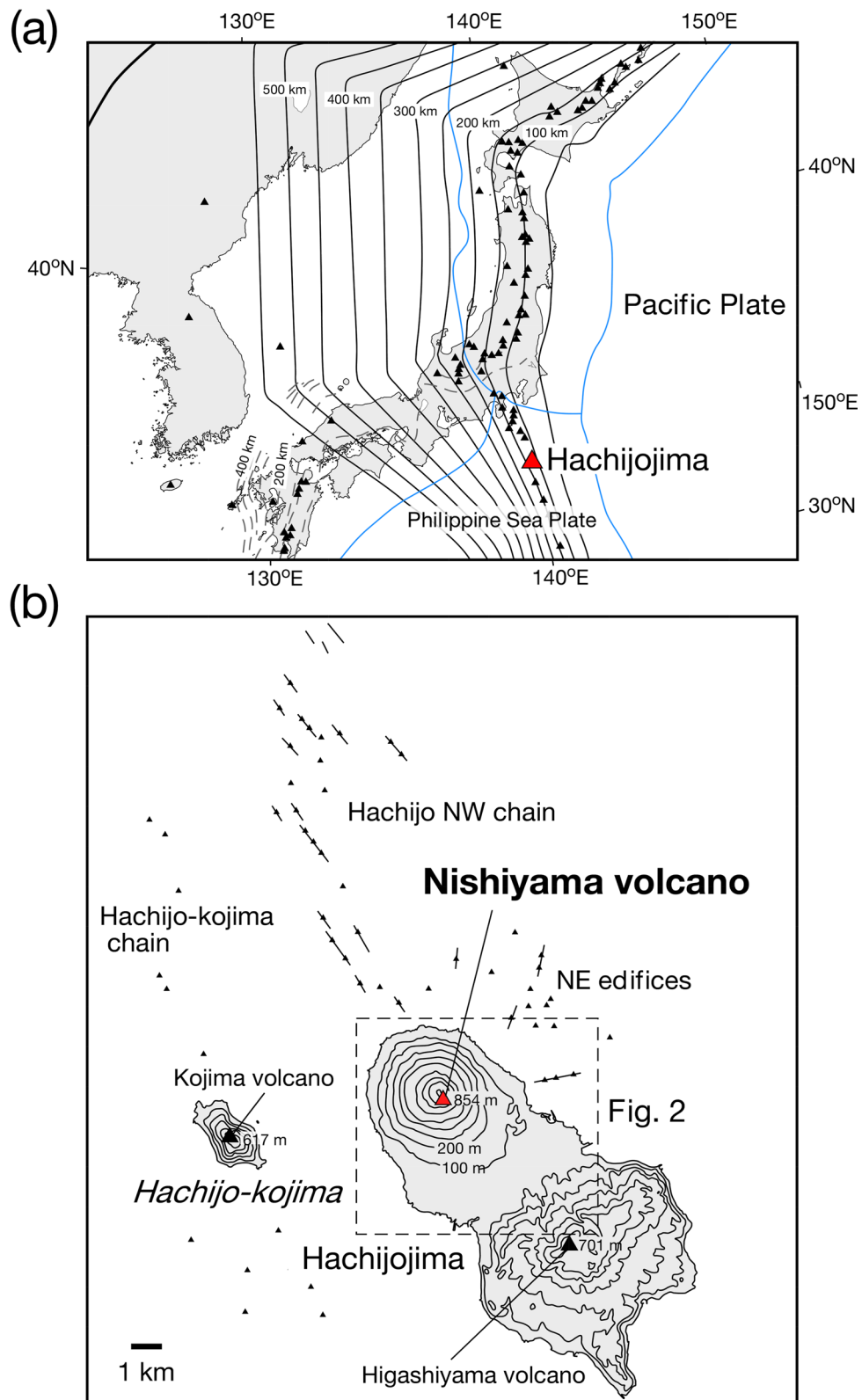


**Fig. 1** (See legend on previous page.)

of the accumulation of plagioclase phenocrysts. We show that the magma plumbing system consisted of a main magma chamber located at a depth of 9–12 km and a deeper magma chamber which was the source of primitive magmas. We further show that the subaerial Nishiyama volcanic products were primarily derived from a single parental magma, but another parental magma was also involved in the magma system before 1 ka. We also suggest that the accumulation and fractionation of plagioclase phenocrysts, which largely control the whole-rock compositional variations of the volcanic products, occurred in the ascending magmas.

### Geological setting

Hachijojima volcano is located on the volcanic front of the Izu–Bonin arc, under which the Pacific plate is subducting (Fig. 1a). The volcano consists of the Nishiyama, Higashiyama, and Kojima volcanoes (Fig. 1b). Geological studies were conducted by Isshiki (1959), Tsukui et al. (1991), Suga (1993, 1994, 1998), Sugihara (1998), and Ishizuka and Geshi (2018). The activity of the Hachijojima volcano began with the formation of the Higashiyama volcano. Kaneoka et al. (1970) reported K–Ar age of <0.14 Ma for older lava from the volcano. The formation of the Higashiyama volcano is considered to have

continued until about 4 ka (Suga 1994). The activity of the Kojima volcano is not well known, but the main edifice is suggested to have been formed by about 3 ka (Ishizuka and Geshi 2018). The Nishiyama volcano has been active since as early as about 10 ka (Tsukui et al. 1991), and its volcanic activity overlapped with later-stage activity of the Higashiyama volcano (Suga 1993).

Ishizuka and Geshi (2018) divided the volcanic activity of Nishiyama into four stages: Mitsune, Senjojiki, Okoshigahana, and Fujitozando (Fig. 2). During the Mitsune stage (10–3 ka), submarine phreatomagmatic eruptions occurred repeatedly, and Nishiyama became a subaerial volcano towards the end of this stage. The eruption products were mainly volcanic breccia and subordinate lavas, including Kandoyama lava (KdL). During the Senjojiki stage (3–1 ka), the main edifice of the Nishiyama volcano was formed by the repeated summit and flank eruptions (SL and SS; Fig. 2). During the Okoshigahana stage (1–0.7 ka), lava flows and pyroclastics were ejected from the summit crater, resulting in Okoshigahana lavas (OkL), Okoshigahana scoria fall (OkS), and Akasari lava (AzL). During the Fujitozando stage (0.7–0.4 ka), summit and flank eruptions occurred repeatedly, generating Debana lava (DbL), Osarigahana lava (OsL), Idesarigahana lava (IdL), Idesarigahanaue lava (IuL), Furiijaen lava

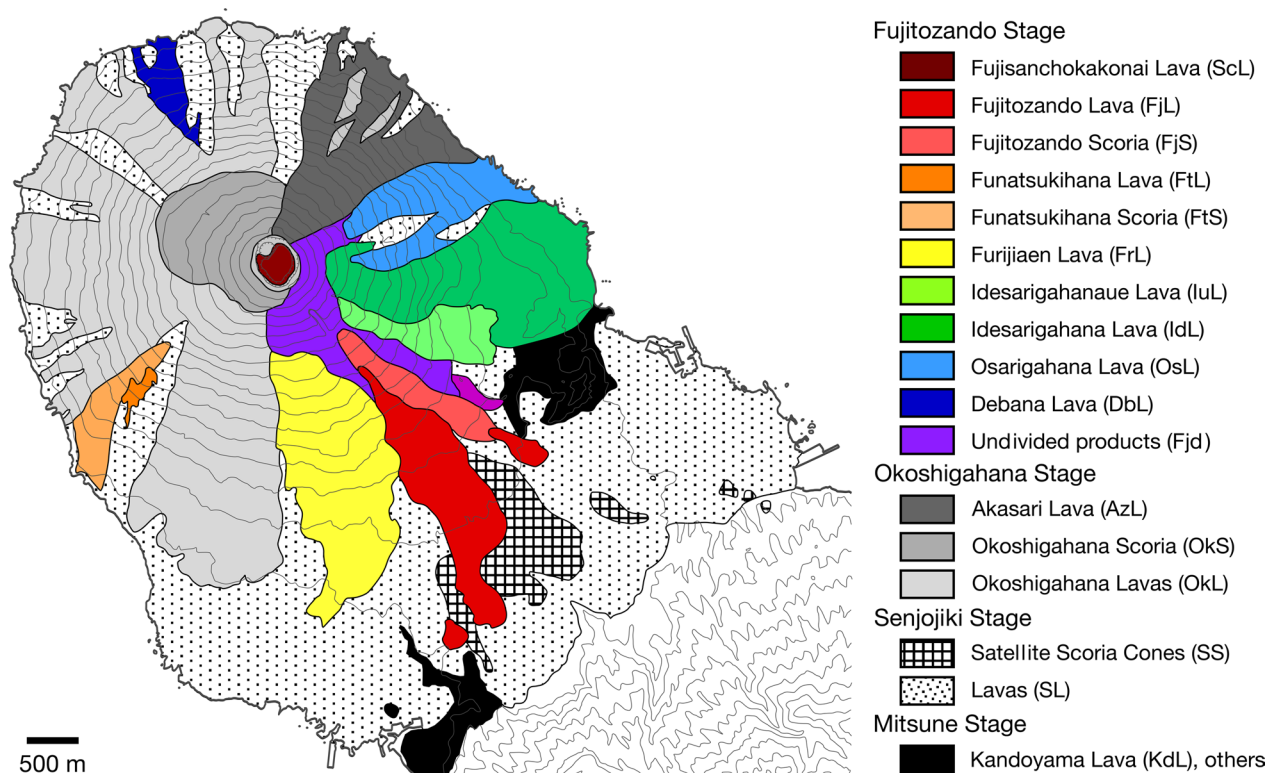


**Fig. 2** Topographic and geologic map of the Nishiyama volcano on Hachijojima Island. The volcanic stratigraphy and the geologic map are from Ishizuka and Geshi (2018)

(FrL), Funatsukihana lava (FtL), Fujitozando scoria cone deposit (FJS), Fujitozando lava (FjL), and Fujisanchokakonai lava (ScL) (Fig. 2). Among these products, FJS and FjL are considered to have been the products of the most recent eruptions in 1605 AD on Hachijojima Island. In addition to these subaerial eruptions, submarine eruptions, that were related to the Nishiyama volcanic activity, occurred along a 20-km-long volcanic chain (“Hachijo NW chain”) and at parasitic cones on the northeastern slope of the Nishiyama volcano (“NE edifice”) (Fig. 1b; Ishizuka et al. 2008).

### Samples and analytical methods

In this study, we investigated the lavas and pyroclastics of subaerial eruptions from the Nishiyama volcano, including those of the Senjojiki, Okoshigahana, and Fujitozando stages (i.e., 3–0.4 ka). Samples from the Kandoyama lava (KdL) of the Mitsune stage were also used for comparison. We collected 238 samples from individual volcanic units, according to the volcanic stratigraphy and geological map of Ishizuka and Geshi (2018). Whole-rock major and trace element analyses using X-ray fluorescence (XRF) spectrometry were performed on all samples. Additional whole-rock trace element analyses using inductively coupled plasma mass spectrometry (ICP-MS) and Sr, Nd, and Pb isotopic analyses were conducted on the representative 25 samples that were selected from the individual volcanic units.

All geochemical analyses were conducted at the Faculty of Science, Hokkaido University, Japan, and the analytical methods were similar to those described by Kuritani et al. (2021a). The lava and scoria samples were crushed into coarse grains with diameters of 3–5 mm and then rinsed with deionized water in an ultrasonic bath for at least 8 h. The washed samples were dried at 110 °C overnight and then pulverized using an alumina rod in a polycarbonate vessel using a Yasui-Kikai Multi-beads shocker<sup>®</sup>. The concentrations of the whole-rock major elements and some trace elements (Sc, V, Cr, Co, Ni, Rb, Sr, Y, Zr, and Ba) were measured via XRF spectrometry using Spectris MagiX PRO. The powdered samples were ignited at 900 °C for >12 h in a muffle furnace. Glass beads were prepared by fusing powdered samples with an alkali flux (2:1 sample dilution) consisting of a 4:1 mixture of  $\text{Li}_2\text{B}_4\text{O}_7$  and  $\text{LiBO}_2$ . The measured compositions of reference material JB-3 (obtained from the Geological Survey of Japan; Imai et al. 1995) and their reference values are listed in Additional file 1: Table S1. The concentrations of additional trace elements were determined using a Thermo Fisher iCAP RQ following the methodology of Yokoyama et al. (2017). To check data quality, the trace element concentrations of JB-3 were also measured under the same conditions, and these concentrations

and their reference values are listed in Additional file 1: Table S2.

Whole-rock Sr, Nd, and Pb isotopic analyses were conducted using a multi-collector (MC)–ICP-MS (Thermo Fisher Scientific Neptune Plus). The analytical procedures for chemical separation followed the methods of Pin et al. (1994) and Noguchi et al. (2011) for Sr, Pin et al. (1994) and Pin and Zalduegui (1997) for Nd, and Kuritani and Nakamura (2002) for Pb. Mass fractionation for Sr and Nd was internally corrected using  $^{86}\text{Sr}/^{88}\text{Sr}=0.1194$  and  $^{146}\text{Nd}/^{144}\text{Nd}=0.7219$ , respectively, and that for Pb was corrected using Tl as an external standard ( $^{205}\text{Tl}/^{203}\text{Tl}=2.3871$ ; Dunstan et al. 1980). Additional corrections were performed by applying a standard bracketing method using NIST987, JNdi-1, and NIST981 for Sr, Nd, and Pb isotopic analyses, respectively, and normalizing to  $^{87}\text{Sr}/^{86}\text{Sr}=0.710240$  for NIST987;  $^{143}\text{Nd}/^{144}\text{Nd}=0.512117$  for JNdi-1; and  $^{206}\text{Pb}/^{204}\text{Pb}=16.9424$ ,  $^{207}\text{Pb}/^{204}\text{Pb}=15.5003$ , and  $^{208}\text{Pb}/^{204}\text{Pb}=36.7266$  for NIST981 (Kuritani and Nakamura 2003). The Sr, Nd, and Pb isotopic ratios of JB-3 measured in this study, reference values, and standard deviations for replicate analyses are provided in Additional file 1: Table S3. The analytical reproducibility ( $2\sigma$ ) for the isotopic analyses of natural samples was typically 0.004% for  $^{87}\text{Sr}/^{86}\text{Sr}$ , 0.002% for  $^{143}\text{Nd}/^{144}\text{Nd}$ , 0.010% for  $^{206}\text{Pb}/^{204}\text{Pb}$ , 0.009% for  $^{207}\text{Pb}/^{204}\text{Pb}$ , and 0.012% for  $^{208}\text{Pb}/^{204}\text{Pb}$ .

The modal compositions of phenocrysts were measured by counting 2000 points per thin section for representative samples. The mineral compositions were determined using a JEOL JXA-8800 electron microprobe. For olivine, clinopyroxene, and orthopyroxene, an accelerating voltage of 15 kV, a beam current of 20 nA, peak and background counting times on each element were 20 and 10 s, respectively, and focused beams were used. For plagioclase, these values were 15 kV, 10 nA, 10 and 5 s, and 10  $\mu\text{m}$ , respectively. Both oxide and natural mineral standards were used, and data were obtained using the ZAF correction method.

### Petrology, geochemistry, and mineralogy

#### Whole-rock compositions

The results of the whole-rock XRF analysis for representative Nishiyama volcanic products are listed in Table 1 and Additional file 1: Table S1 and shown in Fig. 3. The  $\text{SiO}_2$  content of the samples ranges from 49.4–54.9 wt.%, and they can be largely divided into basaltic (<53 wt.%  $\text{SiO}_2$ ) and andesitic samples (>54 wt.%  $\text{SiO}_2$ ), as has been reported by previous studies (Nakano et al. 1991; Tsukui and Hoshino 2002). The andesitic products occurred solely in the SL unit during the Senjojiki stage. The compositional variations of basaltic samples from

**Table 1** Whole-rock compositions of representative samples from the Hachijo-Nishiyama volcano

Sample Unit	#28-1	#55-1	#121-2	#112-1	#89-1	#171-2	#93-1	#2-1	#168-1	#102-1
	KdL	SL	SL	OkL	AzL	DbL	OsL	IdL	FrL	FjS
Major elements, wt.%										
SiO <sub>2</sub>	51.24	51.03	55.08	50.64	50.29	51.88	51.45	50.93	52.78	52.29
TiO <sub>2</sub>	1.42	1.46	1.64	1.41	1.43	1.48	1.67	1.41	1.56	1.48
Al <sub>2</sub> O <sub>3</sub>	16.60	15.31	13.99	16.41	16.96	15.42	14.31	17.28	14.62	15.83
Fe <sub>2</sub> O <sub>3</sub> *	14.15	15.38	14.82	13.81	13.97	14.44	15.99	13.58	14.69	14.31
MnO	0.21	0.23	0.24	0.20	0.20	0.22	0.23	0.20	0.22	0.21
MgO	3.64	4.46	3.16	4.50	4.18	3.89	4.60	4.10	3.76	3.79
CaO	10.14	10.02	7.89	10.62	10.65	9.58	9.39	10.61	9.10	9.57
Na <sub>2</sub> O	2.38	2.07	2.76	2.09	2.06	2.33	2.18	2.13	2.46	2.29
K <sub>2</sub> O	0.33	0.23	0.55	0.34	0.35	0.42	0.44	0.35	0.47	0.43
P <sub>2</sub> O <sub>5</sub>	0.14	0.12	0.23	0.15	0.15	0.17	0.18	0.15	0.17	0.17
Total	100.23	100.32	100.36	100.17	100.26	99.84	100.44	100.74	99.86	100.37
Trace elements, ppm										
Sc**	42.6	49.1	44.2	44.4	43.0	44.0	49.5	41.4	48.1	44.0
V**	481	517	248	396	398	400	448	395	400	397
Cr**	18.8	35.0	4.7	31.8	16.8	15.6	17.8	15.3	17.6	14.4
Co**	43.8	49.3	45.4	45.1	44.8	46.8	49.9	43.9	46.3	45.4
Ni**	17.4	23.8	6.6	18.7	15.7	12.1	16.2	14.8	11.7	11.9
Rb**	6.4	6.7	6.5	7.2	6.8	7.8	7.0	8.4	7.0	7.4
Si**	192	177	193	181	181	176	166	179	176	177
Y**	29.4	28.3	47.6	30.6	31.7	35.5	37.5	31.2	38.2	35.7
Zr**	50.0	45.2	78.6	53.6	54.7	63.2	63.5	53.6	67.7	63.5
Ba**	124	106	201	137	140	166	166	141	176	163
Nb	0.41	0.34	0.65	0.43	0.44	0.51	0.53	0.43	0.54	0.51
Cs	0.42	0.20	0.72	0.46	0.47	0.58	0.63	0.51	0.59	0.61
La	2.51	1.96	4.11	2.58	2.61	3.02	3.18	2.59	3.29	3.03
Ce	7.83	6.3	12.8	8.06	8.17	9.60	10.0	8.21	10.4	9.59
Pr	1.45	1.19	2.39	1.49	1.52	1.77	1.88	1.52	1.93	1.79
Nd	8.65	7.3	14.1	8.86	9.06	10.6	11.1	9.08	11.4	10.6
Sm	3.21	2.84	5.19	3.31	3.37	3.89	4.16	3.40	4.19	3.94
Eu	1.23	1.11	1.75	1.18	1.20	1.33	1.42	1.19	1.39	1.31
Gd	4.68	4.12	7.25	4.73	4.81	5.46	5.78	4.75	5.85	5.47
Tb	0.84	0.75	1.28	0.84	0.85	0.98	1.03	0.85	1.04	0.98
Dy	5.68	5.15	8.68	5.63	5.72	6.56	6.96	5.74	7.03	6.58

**Table 1** (continued)

Sample Unit	#28-1 KdL	#55-1 SL	#121-2 SL	#112-1 OkL	#89-1 AzL	#171-2 DbL	#93-1 OsL	#2-1 IdL	#168-1 FrL	#102-1 Fjs
Ho	1.23	1.10	1.88	1.23	1.24	1.41	1.50	1.24	1.54	1.42
Er	3.68	3.32	5.64	3.68	3.71	4.26	4.52	3.68	4.58	4.28
Tm	0.53	0.49	0.82	0.54	0.54	0.61	0.66	0.54	0.67	0.63
Yb	3.55	3.29	5.47	3.50	3.55	4.17	4.33	3.59	4.49	4.16
Lu	0.53	0.50	0.83	0.53	0.54	0.62	0.66	0.54	0.68	0.62
Hf	1.70	1.53	2.86	1.83	1.85	2.21	2.31	1.87	2.41	2.24
Ta	0.03	0.03	0.05	0.03	0.03	0.04	0.04	0.03	0.04	0.04
Pb	2.45	1.76	3.56	2.38	2.38	3.87	2.80	2.36	2.92	2.76
Th	0.20	0.14	0.33	0.21	0.21	0.25	0.26	0.21	0.27	0.24
U	0.13	0.10	0.20	0.12	0.12	0.15	0.15	0.13	0.17	0.16
<i>Isotopes</i>										
<sup>87</sup> Sr/ <sup>86</sup> Sr	0.703543 ± 8	0.703552 ± 8	0.703543 ± 9	0.703543 ± 12	0.703536 ± 6	0.703552 ± 10	0.703544 ± 13	0.703538 ± 16	0.703537 ± 9	0.703552 ± 13
<sup>143</sup> Nd/ <sup>144</sup> Nd	0.513099 ± 7	0.513099 ± 13	0.513103 ± 5	0.513105 ± 5	0.513103 ± 3	0.513102 ± 5	0.513098 ± 5	0.513099 ± 5	0.513098 ± 3	0.513099 ± 5
<sup>206</sup> Pb/ <sup>204</sup> Pb	18.4080 ± 6	18.4065 ± 6	18.4075 ± 4	18.4110 ± 5	18.4121 ± 4	18.4110 ± 7	18.4108 ± 4	18.4112 ± 6	18.4095 ± 5	18.4089 ± 5
<sup>207</sup> Pb/ <sup>204</sup> Pb	15.5467 ± 6	15.5442 ± 5	15.5453 ± 3	15.5455 ± 6	15.5464 ± 4	15.5468 ± 5	15.5462 ± 4	15.5456 ± 4	15.5464 ± 5	15.5460 ± 4
<sup>208</sup> Pb/ <sup>204</sup> Pb	38.3081 ± 14	38.3011 ± 14	38.3026 ± 9	38.3037 ± 17	38.3074 ± 10	38.3110 ± 14	38.3071 ± 10	38.3058 ± 12	38.3073 ± 15	38.3063 ± 11

Fe<sub>2</sub>O<sub>3</sub>\* total Fe as Fe<sub>2</sub>O<sub>3</sub>

\*\* Obtained by XRF

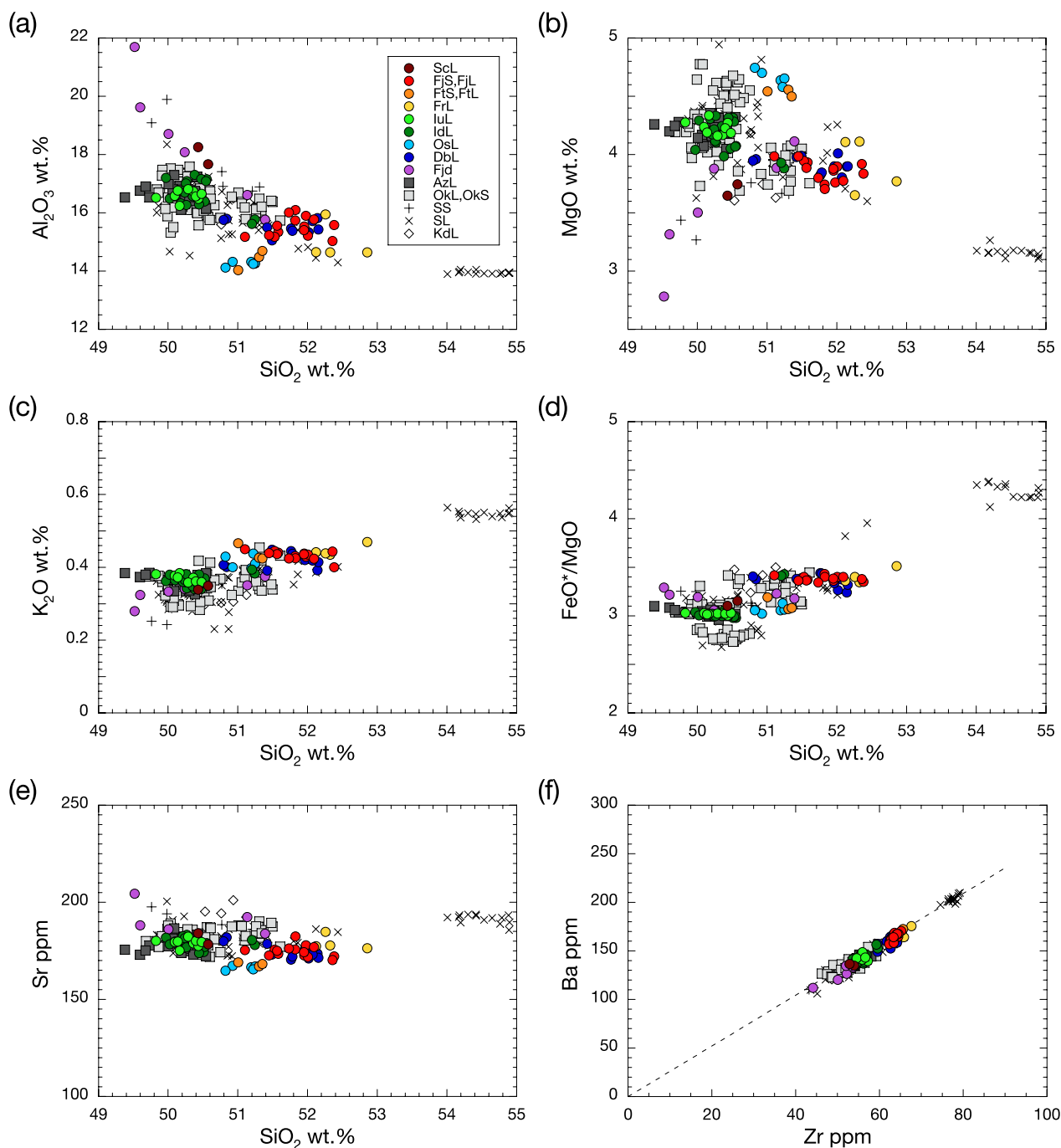


**Fig. 3** SiO<sub>2</sub> variation diagram for **a** Al<sub>2</sub>O<sub>3</sub>, **b** MgO, **c** K<sub>2</sub>O, **d** FeO\*/MgO, and **e** Sr, and **f** Ba–Zr diagram for samples from the Nishiyama volcano. Circles of all colors represent the samples from the Fujitozando stage and squares for the Okoshigahana stage

the Senjojiki (pluses and crosses in Fig. 3), Okoshigahana (squares), and Fujitozando stages (circles) overlap. Although the compositional data are scattered on Harker variation diagrams (Fig. 3a–e), all the data lie on a single line that passes through the origin on the Ba–Zr diagram (Fig. 3f).

The trace element concentration data and Sr, Nd, and Pb isotopic data are listed in Table 1 and Additional file 1: Tables S2 and S3, respectively. A primitive mantle-normalized multi-element diagram of representative samples from the individual volcanic units is shown in Fig. 4a. All the patterns are characterized by

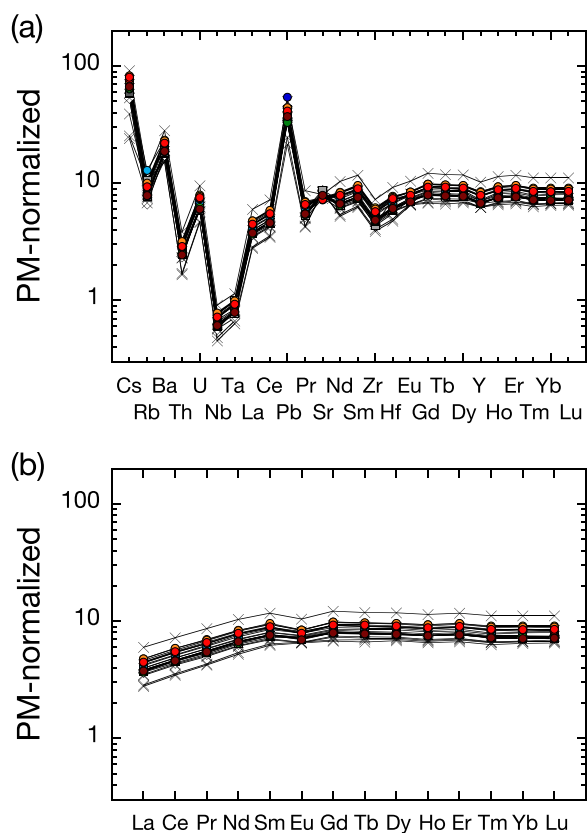


**Fig. 4** **a** Primitive mantle-normalized trace-element concentrations and **b** primitive mantle-normalized rare-earth element concentrations of the representative samples from the Nishiyama volcano. The trace element concentrations of the primitive mantle are taken from Sun and McDonough (1989). Symbols as in Fig. 3

negative anomalies of Nb and Ta and positive spikes in Pb and Sr. These features are characteristic of subduction-related magma. The andesitic sample from the Senjojiki stage (SL) is relatively enriched in the incompatible trace elements. A primitive mantle-normalized rare-earth element (REE) concentration diagram is shown in Fig. 4b. The samples show depletion in light REEs relative to middle and heavy REEs. Weak negative Eu anomalies are observed in all the samples. For the representative samples, the variations in the  $^{87}\text{Sr}/^{86}\text{Sr}$ ,  $^{143}\text{Nd}/^{144}\text{Nd}$ , and  $^{206}\text{Pb}/^{204}\text{Pb}$  isotopic ratios with the  $\text{SiO}_2$  content are shown in Fig. 5. The  $^{87}\text{Sr}/^{86}\text{Sr}$  and  $^{143}\text{Nd}/^{144}\text{Nd}$  ratios of the Nishiyama volcanic products are essentially homogeneous irrespective of the  $\text{SiO}_2$  contents. The  $^{206}\text{Pb}/^{204}\text{Pb}$  ratios of the Nishiyama samples are mostly homogeneous within analytical uncertainty. However, some samples from the Senjojiki stage have slightly lower  $^{206}\text{Pb}/^{204}\text{Pb}$  ratios (Fig. 5c), and the low  $^{206}\text{Pb}/^{204}\text{Pb}$  basaltic samples have low La/Sm ratios (Fig. 5d). We note that these two samples with low  $^{206}\text{Pb}/^{204}\text{Pb}$  and La/Sm ratios have the lowest  $\text{K}_2\text{O}$

contents of about 0.23 wt.% (#55-1; Table 1) among the studied Nishiyama samples.

The temporal variations in the whole-rock compositions of the Nishiyama samples are shown in Fig. 6. The  $\text{FeO}^*/\text{MgO}$  ratios do not exhibit systematic temporal variation, and they show a zig-zag pattern (Fig. 6a). The Zr/Y ratios of the samples from the Fujitozando stage commonly range 1.6–1.9, but some older samples from the Okoshigahana, Senjojiki, and Mitsune stages have relatively lower Zr/Y ratios (Fig. 6b). The two basaltic Senjojiki-stage samples with low  $^{206}\text{Pb}/^{204}\text{Pb}$  and La/Sm ratios (Fig. 5d) also have low Zr/Y ratios of 1.5–1.6. The La/Sm ratios of the samples are homogeneous with 0.75–0.80 except for the two Senjojiki-stage samples (Fig. 6c). Although the  $^{208}\text{Pb}/^{204}\text{Pb}$  ratios of the Nishiyama samples are mostly homogeneous, some older samples have slightly lower  $^{208}\text{Pb}/^{204}\text{Pb}$  ratios (Fig. 6d).

**Petrography and mineralogy**

The phenocryst modal abundances of representative samples of the Nishiyama volcanic products are listed in Additional file 1: Table S4. The phenocryst content of the samples is variable, ranging from 1–40 vol.%. The most abundant phenocryst is plagioclase, and the total amount of mafic phenocrysts (olivine, clinopyroxene, and orthopyroxene) is commonly less than 2 vol.%. The andesite samples from the SL unit are aphyric.

Olivine phenocrysts, up to 0.5 mm in size, are subhedral or anhedral, and they occur as isolated crystals (Fig. 7a). The Fo content [ $100 \times \text{Mg}/(\text{Mg} + \text{Fe})$ ] of the phenocryst cores is 65–66 in sample #8-2 (SL), ~71 in #50-1 (SL), ~69 in #121-2 (SL), 70–71 in #112-2 (OkL), ~68 in #18-1 (OkS), 66–69 in #72-1 (IuL), and 66–67 in #21-1 (FrL). Clinopyroxene phenocrysts, up to 2 mm in length, are commonly euhedral. They rarely occur with orthopyroxene (Fig. 7b) or plagioclase phenocrysts (Fig. 7c). The Mg# [ $100 \times \text{Mg}/(\text{Mg} + \text{Fe})$ ] of the phenocryst cores ranges between 61 and 72 and varies with the samples. Orthopyroxene phenocrysts, up to 2 mm in length, are generally euhedral. Orthopyroxenes rarely form crystal aggregates with plagioclase phenocrysts (Fig. 7d). The orthopyroxene phenocryst cores have Mg# 63–71, which varies with the samples.

Plagioclase phenocrysts, up to ~6 mm in length, are commonly euhedral (Fig. 8). In most samples, the compositions of the plagioclase phenocryst cores normally range from 80–90 in An content [ $100 \times \text{Ca}/(\text{Ca} + \text{Na})$ ], with a mode at 83–85 (Fig. 9). The high-An core regions (>An<sub>80</sub>) contain variable amounts of glass inclusions, ranging from those mostly free from inclusions (Fig. 8a) to those rich in inclusions (Fig. 8b). In some plagioclase phenocrysts, the high-An core region consists of a glass inclusion-poor inner core and an inclusion-rich

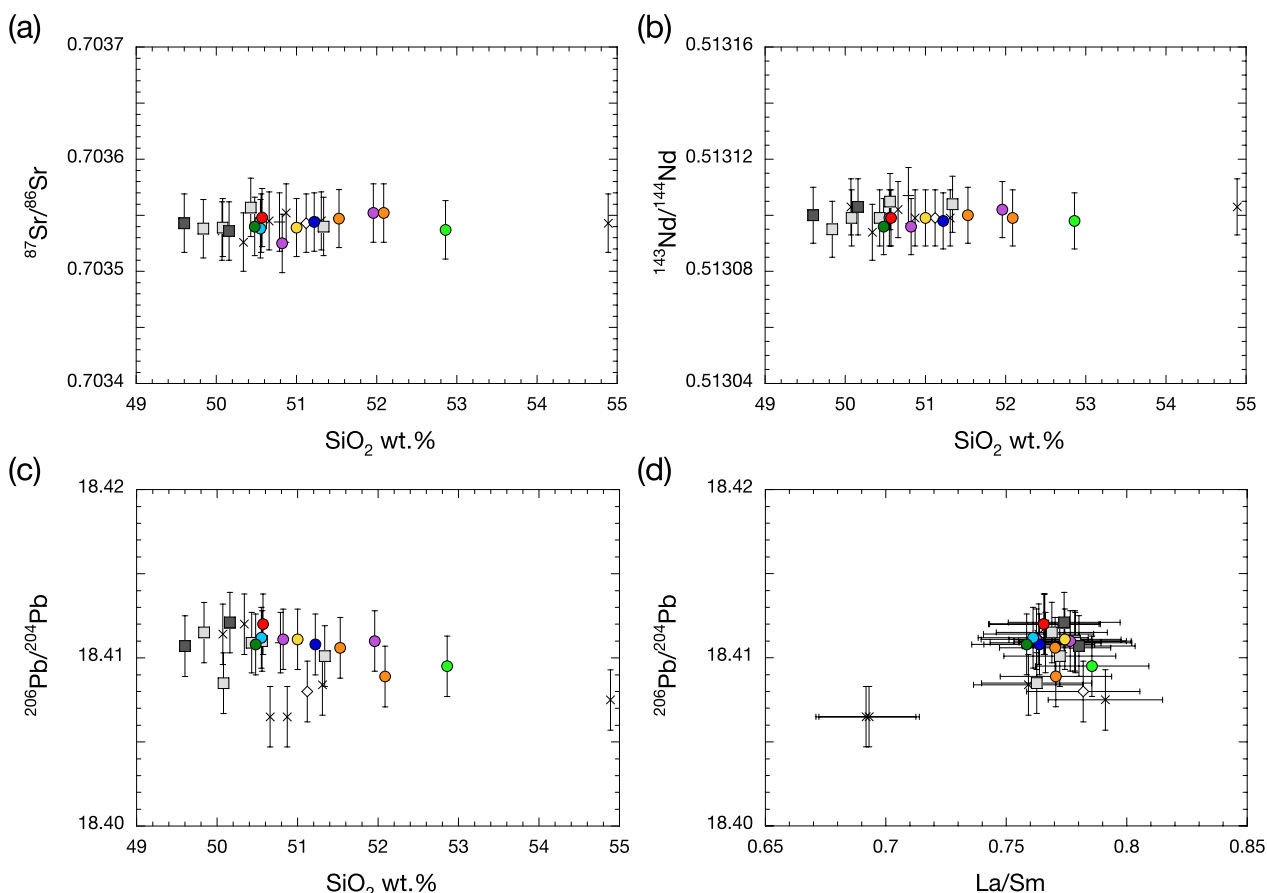


**Fig. 5** SiO<sub>2</sub> variation diagram for **a** <sup>87</sup>Sr/<sup>86</sup>Sr, **b** <sup>143</sup>Nd/<sup>144</sup>Nd, and **c** <sup>206</sup>Pb/<sup>204</sup>Pb, and **d** <sup>206</sup>Pb/<sup>204</sup>Pb vs La/Sm diagram for the representative samples from the Nishiyama volcano. Symbols as in Fig. 3

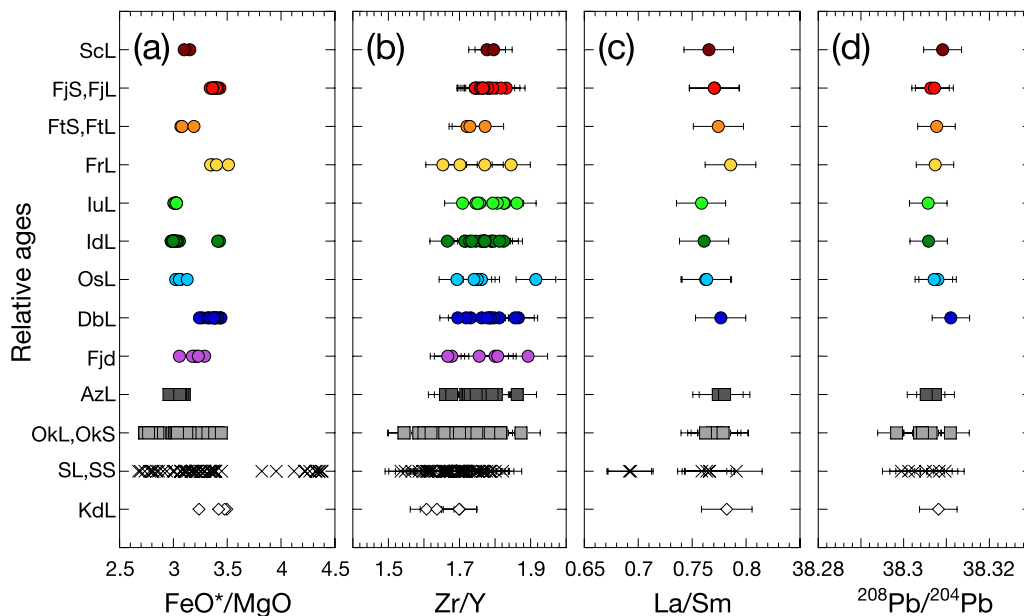


**Fig. 6** The temporal variation of the whole-rock **a** FeO\*/MgO ratios, **b** Zr/Y ratios, **c** La/Sm ratios, and **d** <sup>208</sup>Pb/<sup>204</sup>Pb ratios of the subaerial Nishiyama volcanic products. The vertical axis is not scaled

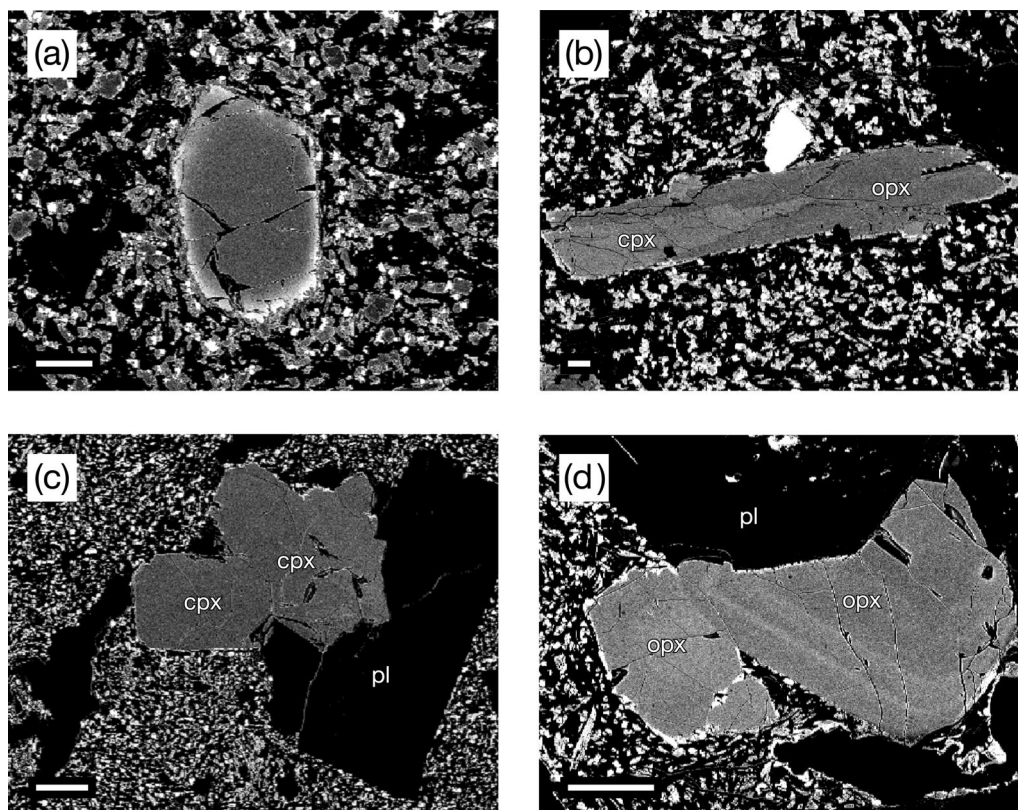


**Fig. 7** Backscattered electron images. **a** Subhedral olivine phenocryst in #112-2 (OkL); **b** crystal consisting of clinopyroxene and orthopyroxene in #136-1 (SL); **c** crystal aggregate consisting of clinopyroxene and plagioclase phenocrysts in #121-2 (SL); **d** crystal aggregate consisting of orthopyroxene and plagioclase phenocrysts in #7-4 (DbL). Abbreviations: ol: olivine, pl: plagioclase, cpx: clinopyroxene, opx: orthopyroxene. The horizontal scale bar represents 0.1 mm

outer mantle (Fig. 8c and d). In some samples, a thick rim ( $>50\ \mu\text{m}$ ) with low An content ( $\text{An}_{65-75}$ ) develops around the core region of the plagioclase phenocrysts (Fig. 8c). Plagioclase microphenocrysts with low An content ( $\text{An}_{65-75}$ ) are present in such samples (Fig. 8c). The thickness of the plagioclase phenocryst rims (i.e., the abundance of low-An plagioclase microphenocrysts) does not depend on the whole-rock composition of the host sample and volcanic stage from which the sample was derived.

## Discussion

### Parental magmas for the Nishiyama volcanic products

The Sr, Nd, and Pb isotopic compositions of the Nishiyama volcanic products, particularly those of the Fujitozando stage, are mostly homogeneous within analytical uncertainty (Fig. 5), but some basaltic samples from the Senjojiki stage have slightly less radiogenic Pb isotopic compositions (Figs. 5c and 6d). These samples are also characterized by lower La/Sm (Fig. 5d) and Zr/Y ratios and lower  $\text{K}_2\text{O}$  contents than those of the other main samples. These observations suggest that the magmas of

the Fujitozando stage were derived from a single parental magma, but another parental magma with distinct compositions (i.e., lower La/Sm, Zr/Y, and Pb isotopic ratios) might have been involved in the Nishiyama magma system before the Fujitozando stage. The presence of multiple primary magmas in a single volcano has also been recognized in other arc volcanoes, such as that of Pagan volcano in the Mariana arc (Tamura et al. 2014) and Meakan volcano in the Kurile arc (Kuritani et al. 2021b).

Ishizuka et al. (2008) suggested that the subaerial Nishiyama volcanic products, as well as submarine products from the Hachijo NW chain and NE edifices (Fig. 1b), were derived from a common primary magma, while some magmas from subaerial satellite cones and those from submarine satellite cones from the NE edifices might have experienced slight crustal assimilation. However, the Hachijo NW chain samples, that are among the most primitive volcanic products in Hachijojima, are characterized by low  $\text{K}_2\text{O}$  contents ( $<0.15\ \text{wt.}\%$ ; Ishizuka et al. 2008). For example, the  $\text{K}_2\text{O}/\text{TiO}_2$  ratios of the most primitive Hachijo NW chain samples are about 0.1 (Ishizuka et al. 2008), which is much lower than those

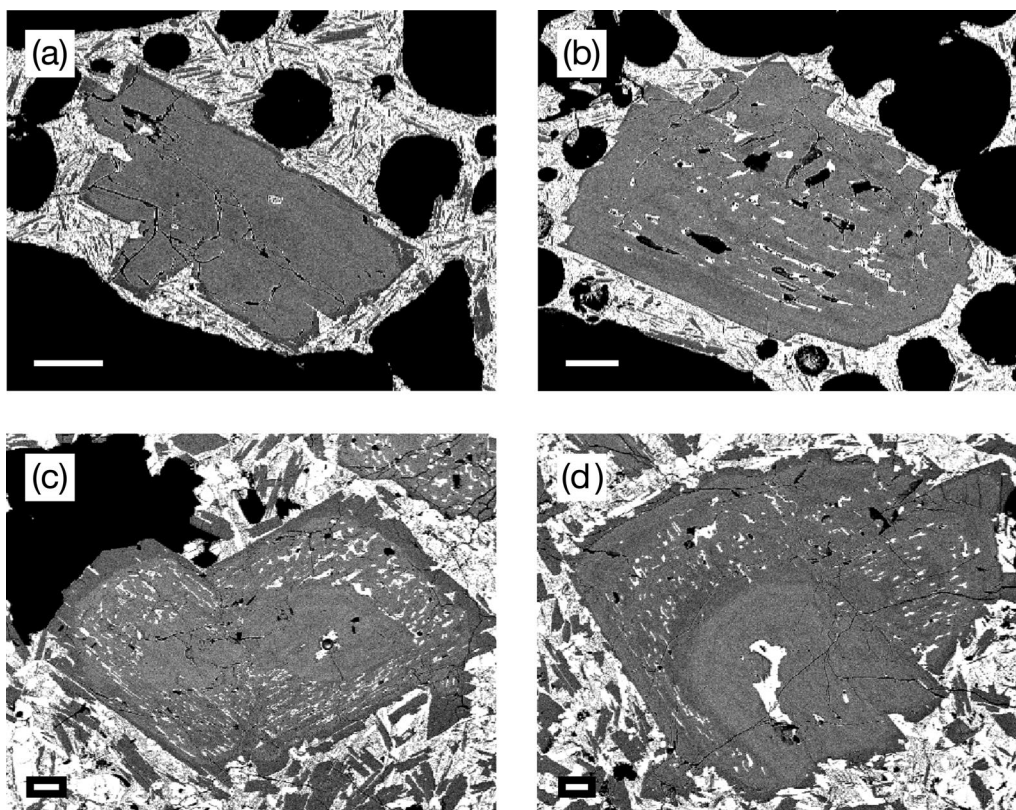


**Fig. 8** Backscattered electron images. **a** Plagioclase phenocryst containing glass inclusion-poor high-An core in #35-1 (FtS); **b** plagioclase phenocryst containing glass inclusion-rich high-An core in #35-1 (FtS); **c, d** plagioclase phenocrysts consisting of inner glass inclusion-poor high-An core, glass inclusion-rich high-An mantle, and low-An rim in #15-2 (ScL). The horizontal scale bar represents 0.1 mm

of the samples from the Fujitozando stage ( $>0.24$ ; Additional file 1: Table S1). Considering that titanomagnetite phenocryst is absent in the mafic Nishiyama samples, it is unlikely that the Fujitozando-stage magmas with the  $K_2O/TiO_2$  ratios of  $>0.24$  were derived from the primitive Hachijo NW chain magma with the  $K_2O/TiO_2$  ratios of 0.1. Therefore, we concluded that the parental magma for the Fujitozando-stage samples was different from that for the Hachijo NW chain samples.

As discussed above, the lower La/Sm, Zr/Y, and Pb isotopic ratios of some Senjojiki-stage samples (Fig. 5d) might have been attributed to the involvement of another parental magma in the Nishiyama magma system. Considering that these samples have the lowest  $K_2O/TiO_2$  ratios of  $\sim 0.16$  among the subaerial Nishiyama samples, the parental magma for these samples, which is expected to have low- $K_2O$  content and low Zr/Y and La/Sm ratios, might have been similar to the primitive Hachijo NW chain magma with the  $K_2O/TiO_2$  ratios of 0.1. This scenario is consistent with the observations that the primitive Hachijo NW chain samples have lower Zr/Y ratios of about 1.3 and lower La/Sm ratios of about 0.6

(Ishizuka et al. 2008) than those of the subaerial Nishiyama samples.

#### Origin of whole-rock compositional variation

The whole-rock compositions of the samples collected from the Nishiyama volcano are variable (49.4–54.9 wt.%  $SiO_2$ ) and are scattered on Harker variation diagrams (Fig. 3). However, except for some low-Zr/Y samples, the Nishiyama magmas, particularly those of the Fujitozando stage, were derived from a single parental magma and that compositional variations were established essentially by crystal–melt separation, without a significant contribution from crustal assimilation. If the Nishiyama magmas were differentiated by a series of fractional crystallization in a single magma chamber, the compositional evolution would have followed a single liquid line of descent. Therefore, the scattered compositional data on Harker variation diagrams suggest that the formation of compositional variations involved multiple processes occurring at different depths.

Figure 10 shows the whole-rock compositions of the Nishiyama samples in the  $Al_2O_3$ –MgO diagram. In the figure, the compositions of some volcanic units, such as

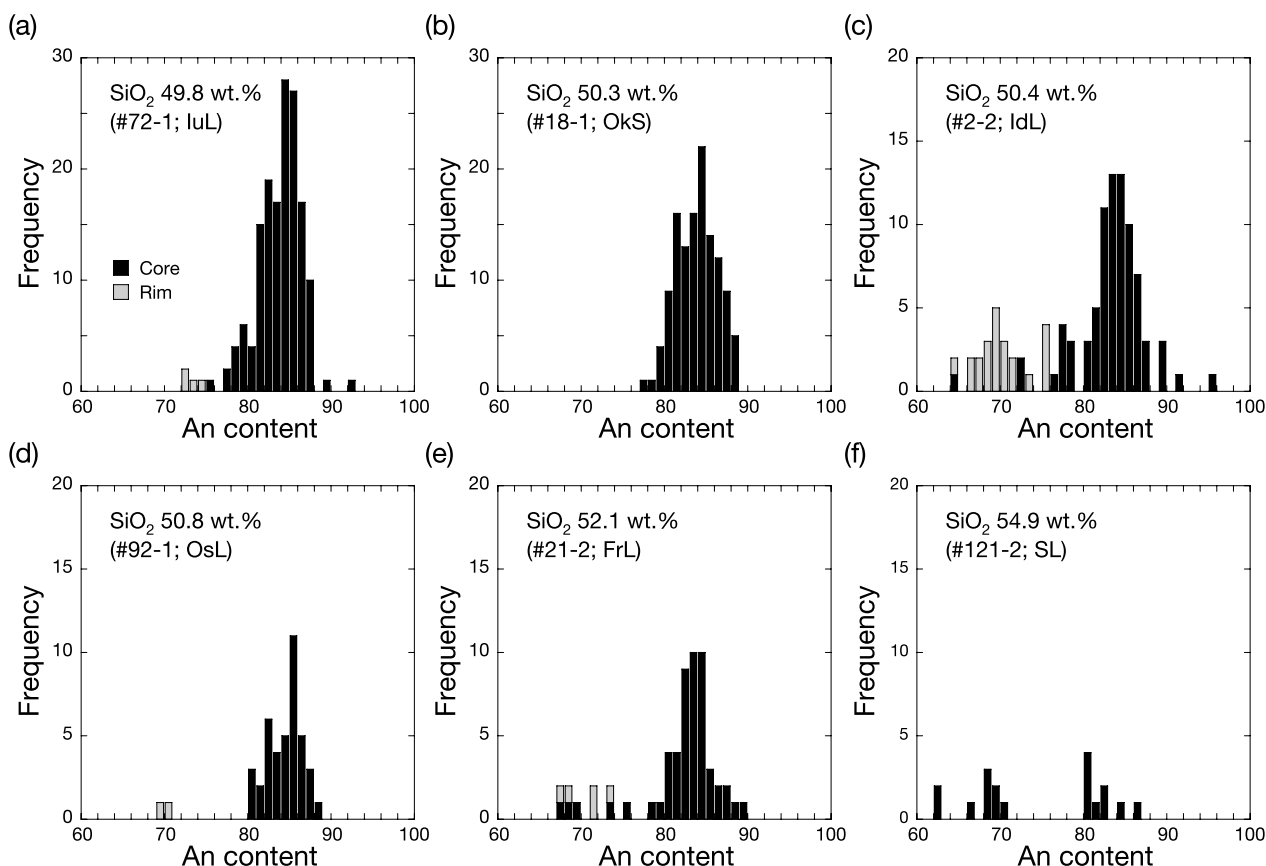


**Fig. 9** Histograms of An content of plagioclase phenocryst and microphenocryst cores and rims for the representative samples from the Nishiyama volcano

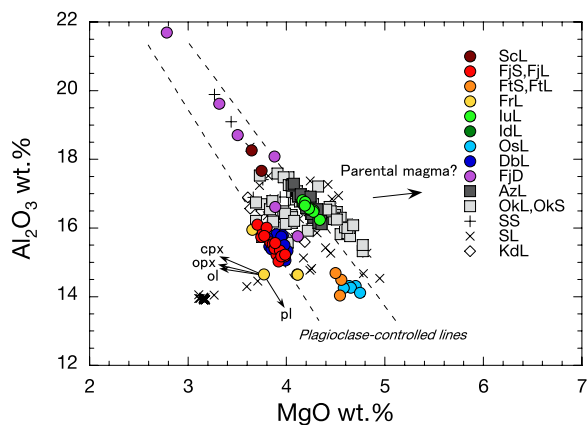


**Fig. 10**  $Al_2O_3$ –MgO diagram for the subaerial Nishiyama volcanic products. For sample #168-1 (FrL), the compositional vectors resulting from the fractionation of olivine (ol), clinopyroxene (cpx), orthopyroxene (opx), and plagioclase (pl) are shown

FjS–FjL, luL, FjD, AzL, and a part of OkS–OkL, exhibit tight linear trends that correspond to plagioclase-controlled lines (broken lines in Fig. 10). This observation

suggests that the trends were primarily established by the accumulation or fractionation of plagioclase phenocrysts (Nakano et al. 1991; Tsukui and Hoshino 2002; Aizawa et al. 2020). This is supported by the observation that the whole-rock  $FeO^*/MgO$  ratios, which do not change with fractionation or accumulation of plagioclase, are mostly constant for some units, irrespective of the  $SiO_2$  content (Fig. 3d). The subaerial Nishiyama magmas are significantly differentiated from mantle-derived primary magma because of the low MgO contents (< 5 wt.%). This observation, along with the tight plagioclase-controlled trends, suggests that magmatic differentiation from the parental magma was followed by the accumulation or fractionation of plagioclase phenocrysts.

**Depth of magma chamber**

As discussed above, the compositional variations of the subaerial Nishiyama products were essentially established by crystal–melt separation. Therefore, there must have been a magma chamber in which differentiation from the parental primitive magma to the magmas of the subaerial volcanic products occurred. To estimate

the depth of the magma chamber, the crystallization pressures of the pyroxene phenocrysts were estimated by applying the two-pyroxene geothermobarometer of Putirka (2008) to the clinopyroxene–orthopyroxene pairs found in three samples (#121-2, SL; #7-4, DbL; and #101-1, FjS; Additional file 1: Table S5). The clinopyroxene–orthopyroxene pairs in #121-2 and #7-4 show evidence of contemporaneous growth, but crystal aggregates consisting of orthopyroxene and clinopyroxene were not found in #101-1. Therefore, for this sample, the pressure conditions were estimated using the core compositions of the euhedral clinopyroxene and orthopyroxene phenocrysts in the same thin section. The Fe–Mg exchange coefficients  $K_D(\text{Fe–Mg})^{\text{cpx–opx}}$  are all within the range of  $1.09 \pm 0.14$  (Additional file 1: Table S5), which ensures that the pyroxene pairs were in equilibrium (Putirka 2008).

The result shows that the pressure conditions for the pyroxene crystallization in the samples range 3–4 kbar (Fig. 11). Considering the typical uncertainty of this method of 2.8 kbar (Putirka 2008), the difference in the estimated pressure conditions of the three volcanic stages is not significant. Therefore, we suggest that the magma chamber in which pyroxene crystallization occurred was located at 3–4 kbar, equivalent to a depth of 9–12 km. Ishizuka et al. (2008) considered that the magma plumbing system at the Nishiyama volcano consists of a deep magma chamber (>20 km depth) from which the main parental magmas were supplied, a middle magma chamber (10–20 km depth) from which the Hachijo NW chain magmas branched off, and a shallow magma chamber (<5 km depth) in which crystal fractionation and plagioclase accumulation occurred. In this case, the magma chamber located at a depth of 9–12 km, the presence of

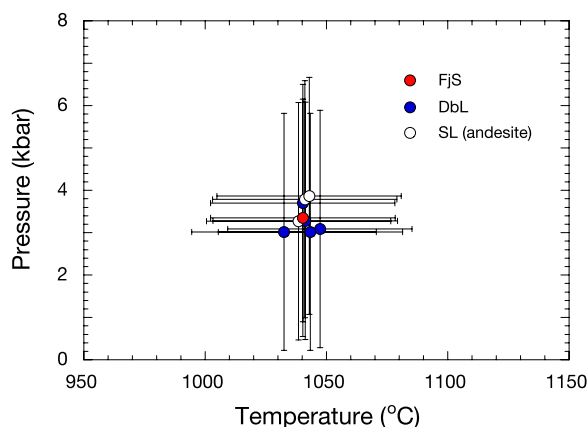


**Fig. 11** The crystallization pressures and temperatures for the pyroxene phenocrysts in the samples (#101-1, #7-4, and #121-2) from FjS, DbL, and SL units estimated using the two-pyroxene geothermobarometer of Putirka (2008)

which is suggested by the pyroxenes in this study, may correspond to the middle magma chamber of Ishizuka et al. (2008). Ishizuka et al. (2008) estimated the depth of the middle magma chamber based on the depth range of the earthquake swarms that occurred in 2002 (Kimata et al. 2004). The estimated magma chamber depth of 9–12 km is also consistent with the dike injection depth of about 12 km estimated from the geodesic ground deformation (Kimata et al. 2004).

The water content of melt in the magma chamber at a depth of 9–12 km was estimated for sample #7-4 (DbL) which was used above. The melt composition was calculated using the whole-rock composition (Additional file 1: Table S1) and phenocryst modal abundances (Additional file 1: Table S4), assuming the average An content of plagioclase phenocrysts of 83 and the Mg# of orthopyroxene phenocrysts of 70. The water content was estimated using the constraint that the melt was saturated with plagioclase at 1030 °C and 3 kbar (obtained above from the two-pyroxene geothermobarometry), and the water content of 4 wt.% was obtained using Eq. 26 of Putirka (2008).

#### Crystallization of plagioclase phenocrysts

Previous petrological studies on Nishiyama volcanic products have suggested that crystal–melt separation involving high-An plagioclase phenocrysts (>An<sub>80</sub>) played a primary role in producing the whole-rock compositional variations of the Nishiyama products (e.g., Nakano et al. 1991; Tsukui and Hoshino 2002; Aizawa et al. 2020). In this section, the origin and crystallization processes of plagioclase phenocrysts are discussed.

Aizawa et al. (2020) recently suggested that the high-An plagioclase phenocrysts formed primarily in a shallow-level magma chamber at <5 km depth under supersaturated conditions by increasing the liquidus temperatures due to decompression-induced vapor exsolution from the melt. However, we found that high-An plagioclase phenocrysts in some subaerial Nishiyama samples show evidence of simultaneous growth with pyroxene phenocrysts (Fig. 7a and d). Because the pyroxene phenocrysts crystallized at 9–12 km depth (Fig. 11), high-An plagioclase crystals are suggested to have been present in the middle-crustal magma chamber.

In some plagioclase phenocrysts, a glass inclusion-poor inner-core region is mantled by a glass inclusion-rich region (Fig. 8c and d). Such glass inclusion-rich plagioclase crystals can be formed by either rapid growth (honeycomb texture) or partial dissolution (dusty texture) of the crystals (e.g., Kawamoto 1992). The size of the glass inclusions in the plagioclase phenocrysts from the Nishiyama volcano is larger than those of plagioclase formed by partial dissolution experiments, which are

characterized by fine glass inclusions (e.g., Tsuchiyama 1985; Nakamura and Shimakita 1998). In addition, if the glass inclusion-rich mantle was formed by partial dissolution, the dissolution should invade the inner glass inclusion-poor core region. However, the inner cores always show euhedral outlines (Fig. 8c and d), and no glass inclusions that cut the outlines of the inner cores are found. Therefore, it is suggested that the glass inclusion-rich mantle was formed by rapid overgrowth of the inner-core plagioclase. In this case, the change in the texture within the individual plagioclase phenocrysts (Fig. 8c and d) suggests that there were at least two growth stages; plagioclase formed under a relatively static condition (i.e., glass inclusion-poor inner core) followed by rapid overgrowth under a supersaturated conditions to form the glass inclusion-rich mantle. Considering that glass inclusions are rare in plagioclase phenocrysts that coexist with pyroxene phenocrysts (Fig. 7c and d), it is likely that the inclusion-poor plagioclase crystals formed in the magma chamber at a depth of 9–12 km. On the other hand, the rapid growth of plagioclase is likely to have occurred during magma ascent by increasing the liquidus temperatures due to water exsolution from the melt (e.g., Kuritani 1999; Taniuchi et al. 2021), as discussed by Aizawa et al. (2020).

As estimated above, the H<sub>2</sub>O content of the melt in some Nishiyama magmas was about 4 wt.% in the magma chamber at a depth of 9–12 km. Considering that the water solubility in the basaltic melt is approximately 4 wt.% at 1.6 kbar (Newman and Lowenstern 2002), the degassing-induced rapid overgrowth of plagioclase phenocrysts is considered to have occurred in the magmas at shallower depths than 5 km.

#### Accumulation of plagioclase phenocrysts

Ishizuka et al. (2008) and Aizawa et al. (2020) considered that the accumulation of plagioclase phenocrysts occurred in a shallow magma chamber located at <5 km depth; however, neither explicitly discussed how the depth of <5 km was constrained. If the magmas resided in a static magma chamber, it is expected that overgrowth of the phenocrysts would have occurred there. In some samples, plagioclase phenocrysts have thick rims with low An content surrounding the high-An core regions (Fig. 8c). It is unlikely that thick rims developed during cooling after the eruption, because rims are also found in quenched scoria samples. Therefore, the thick low-An rims would have grown during storage in a shallow magma chamber. However, in many other samples considered to have experienced plagioclase accumulation, thick rims are not present in the plagioclase phenocrysts (Fig. 8b). This contradicts the inference that accumulation of plagioclase occurred in a static magma chamber.

The presence of a shallow-level static magma chamber is also questioned by the variations in whole-rock compositions among the subaerial Nishiyama volcanic products, which consist of several discrete groups exhibiting tight plagioclase-controlled trends in the Al<sub>2</sub>O<sub>3</sub>–MgO diagram (Fig. 10). If plagioclase accumulation occurred in a static magma chamber at shallow levels, convection must not have been effective, because the homogenization of the magmas resulting from the convective current would have inhibited the accumulation or fractionation of plagioclase phenocrysts. Without vigorous convection, when a new magma is injected into the magma chamber in which the magmas exhibiting plagioclase-controlled compositional variation reside (Fig. 12a), the magmas would not mix effectively. The heterogeneous mixing between the two magmas and the subsequent plagioclase accumulation or fractionation would result in the formation of a compositional area in the Al<sub>2</sub>O<sub>3</sub>–MgO diagram (Fig. 12b and c), instead of the compositional groups with distinct plagioclase-controlled trends (Figs. 10 and 12d).

Based on these considerations, we conclude that a static magma chamber was not present at shallow levels (<5 km) beneath the Nishiyama volcano. Alternatively, we suggest that plagioclase accumulation and fractionation occurred in the magmas during ascent (Fig. 13). This scenario can explain the observed whole-rock compositional variations of the subaerial Nishiyama samples (i.e., consisting of discrete compositional groups with tight plagioclase-controlled trends; Fig. 12d), because each magma batch with a distinct composition (i.e., Al<sub>2</sub>O<sub>3</sub>/MgO ratio), ascending from the 9–12 km magma chamber to the surface, did not necessarily interact with each other before plagioclase fractionation and accumulation. The absence or presence of the thick rims of the plagioclase phenocrysts can also be explained by different ascent paths: magma batches that temporarily stalled during the ascent may have resulted in the formation of plagioclase rims, whereas those that ascended without stalling for a significant time did not develop thick rims (Fig. 13).

Figure 14 compares the density of the melt with that of plagioclase with An<sub>80–92</sub>. The melt was represented by the interstitial melt of sample #7-4 (Additional file 1: Table S1), as used above. The variation in the melt density with pressure was calculated using the model of Iacovino and Till (2019) assuming that the temperature was constant at 1030 °C (obtained above from the two-pyroxene geothermometry). As discussed above, the water content of the melt was about 4 wt.%, and the melt was saturated with water at about 1.6 kbar. The H<sub>2</sub>O content of the water-saturated melt as a function of pressure was obtained using the water solubility model of Newman and Lowenstern (2002). The density of plagioclase with

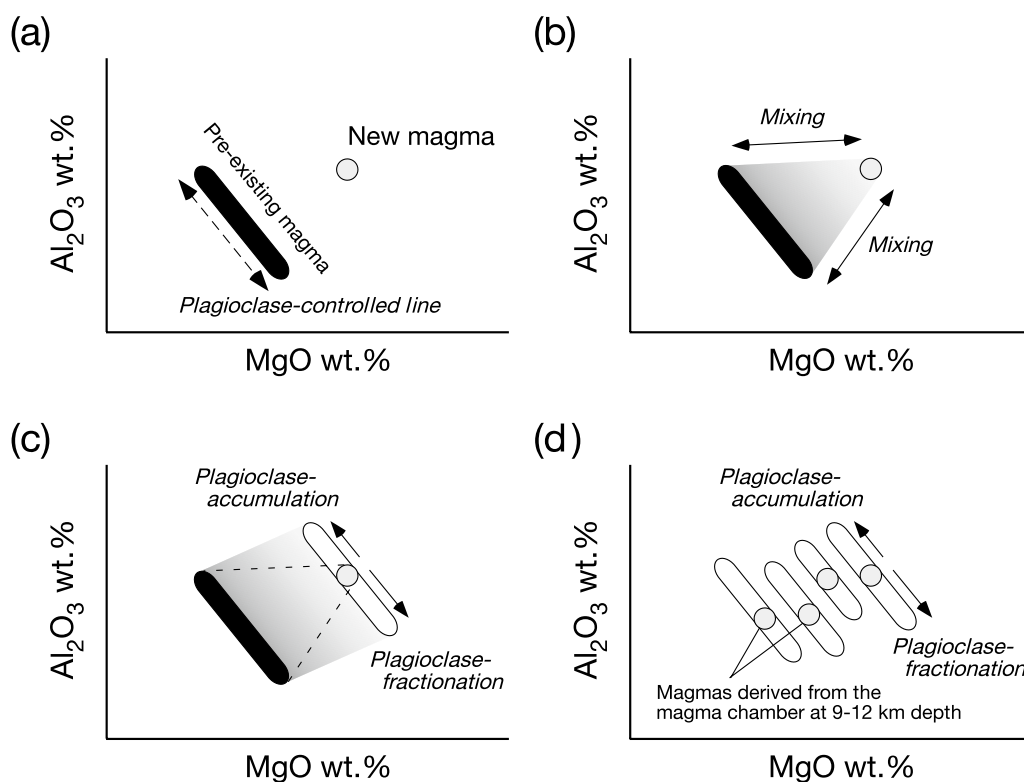


**Fig. 12** Schematic illustration showing the formation of a compositional variation by magma mixing in the  $Al_2O_3$ – $MgO$  diagram. See text for details

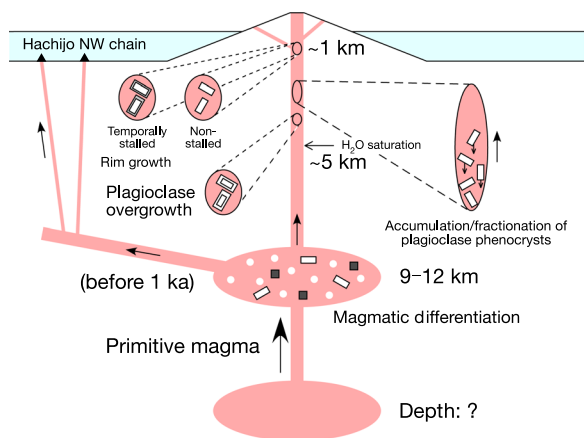


**Fig. 13** Schematic illustration showing the magma plumbing system and pre-eruption magmatic processes at the Nishiyama volcano

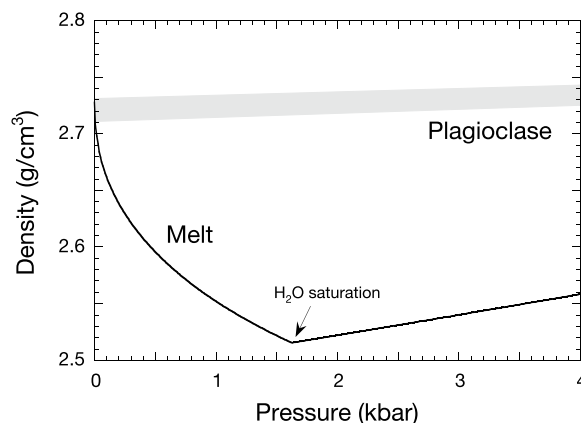


**Fig. 14** Calculated variations in the densities of the melt and plagioclase with pressure. The dry melt composition is represented by the groundmass composition of sample #7-4 (Additional file 1: Table S1). The densities of the melt and plagioclase were calculated using the models of Iacovino and Till (2019) and Berman (1988), respectively

$An_{80-92}$  at 1030 °C as a function of pressure was calculated using the model and parameters of Berman (1988). The comparison shows that the density of plagioclase was higher than that of the melt at < 4 kbar (Fig. 14). This suggests that, during the ascent of magma from the 9–12 km magma chamber, plagioclase phenocrysts would not have floated in the melt. Thus, accumulating and fractionating plagioclase settled relative to the surrounding melt as the

melt ascended (Fig. 13). Effective plagioclase–melt separation might have occurred at deeper levels, where the density difference between the melt and plagioclase was larger. For example, the simple Stokes’s law suggests that a hypothetical spherical plagioclase crystal with a radius

of 2 mm would settle at a velocity of 1.3 m/d at 1030 °C and 1.5 kbar, where the melt water content is estimated to be 3.8 wt.% and the melt viscosity is calculated to be  $10^{2.0}$  Pa·s (using the model of Giordano et al. 2008). As plagioclase phenocrysts settled in an ascending magma batch, it is expected that the abundance of plagioclase phenocrysts in the magmas would increase as the eruption progresses. Unfortunately, however, we could not successfully test this hypothesis because each volcanic unit (Fig. 2) commonly consists of many lava flow units and it was difficult to determine the eruption sequence of individual samples collected from the each volcanic unit.

### Magma plumbing system

The magma plumbing system and pre-eruption magmatic processes inferred from the results of this study are summarized in Fig. 13. Parental magmas for the Nishiyama volcano were homogeneous during the Fujitozando stage (<0.7 ka), while another parental magma with distinct geochemical features, which may have erupted from the Hachijo NW chain, was also present in the magmatic system before 1 ka. The parental primitive magmas were supplied from deep levels to the magma chamber at a depth of 9–12 km. Magmatic differentiation resulting from the fractional crystallization of olivine, pyroxenes, and plagioclase occurred in the magma chamber. The temporal variation in the whole-rock Fe<sup>\*</sup>/MgO ratios, that are not affected by plagioclase accumulation and fractionation, is rather complex, and the ratios do not increase systematically with time (Fig. 6a), suggesting that primitive magmas were intermittently supplied to the magma chamber in which fractional crystallization occurred. During the ascent of magmas from the magma chamber, significant overgrowth of plagioclase phenocrysts is suggested to have occurred at levels shallower than about 5 km. And then, gravitational plagioclase–melt separation occurred in the ascending magmas, resulting in the accumulation and fractionation of plagioclase phenocrysts in the magmas.

Some magmas are considered to have stalled temporarily during their ascent to the surface, resulting in the crystallization of the microphenocrysts and thick rims of the plagioclase phenocryst (Fig. 8c). For sample #7–4, the pressure conditions for the crystallization were estimated assuming that the interstitial melt (Additional file 1: Table S1) was in equilibrium with An<sub>69</sub> plagioclase (the mode of the An content of the rims; Fig. 9) at 1030 °C. The plagioclase–melt hygrometer (Eq. 25b of Putirka 2008) yields a melt H<sub>2</sub>O content as 1.8 wt.%. Because the melt was saturated with H<sub>2</sub>O at shallow levels, as discussed above, the pressure was estimated to be about 0.3

kbar using the water solubility model of Newman and Lowenstern (2002). Therefore, it is suggested that the magmas stalled temporarily at a depth of approximately 1 km (Fig. 13).

### Conclusions

To understand the pre-eruption magmatic processes and magma plumbing system at the Nishiyama volcano on Hachijojima Island, we conducted petrological and geochemical analyses of mafic products from the volcano and arrived at the following conclusions:

- 1) The whole-rock Sr, Nd, and Pb isotopic compositions of the samples from the Fujitozando stage (<0.7 ka) are homogeneous, suggesting that the magmas were derived from a single parental magma and that the variations in the whole-rock major and trace element contents were produced essentially by crystal–melt separation.
- 2) Some samples from the Senjojiki stage (1–3 ka) have lower K<sub>2</sub>O/TiO<sub>2</sub>, Zr/Y, La/Sm, and Pb isotopic ratios than those of the other main samples. This observation suggests that another parental magma with different geochemical features from those of the parental magma for the Fujitozando stage was present before 1 ka. This parental magma may have been similar to the primitive magmas erupted from the Hachijo NW chain.
- 3) The magma plumbing system consisted of a middle-crustal magma chamber located at a depth of 9–12 km and a deeper magma chamber which was likely the source of primitive magmas. Magmatic differentiation occurred primarily in the middle-crustal magma chamber, into which primitive magmas were intermittently injected.
- 4) Plagioclase phenocrysts crystallized in the middle-crustal magma chamber and as the magma ascended from this magma chamber. The accumulation and fractionation of plagioclase phenocrysts, which largely control the whole-rock compositional variations of the subaerial Nishiyama volcanic products, occurred in the ascending magmas, probably at relatively deep levels. Some magmas are suggested to have stalled at a depth of about 1 km, resulting in the crystallization of microphenocrysts and thick rims surrounding the plagioclase phenocrysts.
- 5) The estimated depth of 9–12 km for the middle-crustal magma chamber coincides well with the range of depths over which earthquake swarms occurred in 2002, suggesting that the magma chamber is still active. The earthquake swarms may have been caused

by the injection of primitive magma into the magma chamber.

## Supplementary Information

The online version contains supplementary material available at <https://doi.org/10.1186/s40623-022-01761-9>.

**Additional file 1: Table S1.** Results of the XRF analyses for representative samples from the Hachijo-Nishiyama volcano. **Table S2.** Results of the ICP-MS analyses for a subset of 25 selected samples from the Hachijo-Nishiyama volcano. **Table S3.** Results of the Sr-Nd-Pb isotopic analyses for a subset of 25 selected samples from the Hachijo-Nishiyama volcano. **Table S4.** Modal compositions of representative samples from the Hachijo-Nishiyama volcano. **Table S5.** Temperature and pressure conditions estimated using the two-pyroxene geothermobarometry.

### Acknowledgements

We are grateful to Dr. Akiko Matsumoto for helping us with XRF and EPMA analyses. Fruitful and constructive comments by two anonymous reviewers substantially improved the manuscript. We also thank Professor Katsuya Kaneko for editorial handling.

### Author contributions

MN conceived this study. KO and MN collected the rock samples, and KO, TK, and SY conducted the analyses. All authors contributed to the interpretation of the data. KO and TK led the manuscript preparation efforts with input from MN and SY. All authors read and approved the final manuscript.

### Funding

This work was supported by research grants from the Japan Society for the Promotion of Science Grants-in-Aid for Scientific Research to TK (Grant Number 20H02001) and by the Ministry of Education, Culture, Sports, Science and Technology (MEXT) of Japan, under the Second Earthquake and Volcano Hazards Observation and Research Program (#HKD\_02) and the Integrated Program for Next Generation Volcano Research and Human Resource Development.

### Availability of data and materials

All data generated and/or analyzed during this study are included in this published article and its Additional file.

### Declarations

### Competing interests

The authors declare that they have no competing interests.

### Author details

<sup>1</sup>Graduate School of Science, Hokkaido University, Sapporo 060-0810, Japan. <sup>2</sup>Present Address: Kumagai Gumi Co., Ltd, Tokyo 162-8557, Japan. <sup>3</sup>Faculty of Science, Hokkaido University, Sapporo 060-0810, Japan.

Received: 19 August 2022 Accepted: 28 December 2022

Published online: 16 January 2023

### References

- Aizawa M, Saito T, Imura T, Yasui M (2020) Anorthositic products from the Hachijo-jima island, Izu-Bonin arc: the direct evidence for 'plagioclase control' in shallow magma reservoir. *J Mineral Petrol Sci* 115:375–390
- Berman RG (1988) Internally-consistent thermodynamic data for minerals in the system  $K_2O$ - $Na_2O$ - $CaO$ - $MgO$ - $FeO$ - $Fe_2O_3$ - $Al_2O_3$ - $SiO_2$ - $TiO_2$ - $H_2O$ - $CO_2$ . *J Petrol* 29:445–522
- Dunstan LP, Gramlich JW, Barnes IL (1980) Absolute isotopic abundance and the atomic weight of a reference sample of thallium. *J Res Nat Bureau Standards* 85:1–10
- Giordano D, Russell JK, Dingwell DB (2008) Viscosity of magmatic liquids: a model. *Earth Planet Sci Lett* 271:123–134
- Iacovino K, Till CB (2019) DensityX: a program for calculating the densities of magmatic liquids up to 1627 °C and 30 kbar. *Volcanica* 2:1–10
- Imai N, Terashima S, Itoh S, Ando A (1995) 1994 compilation values for GSJ reference samples, "Igneous rock series." *Geochem J* 29:91–95
- Ishizuka O, Geshi N, Itoh J, Kawanabe Y, TuZino T (2008) The magmatic plumbing of the submarine Hachijo NW volcanic chain Hachiojima, Japan: long-distance magma transport? *J Geophys Res* 113:B08S08
- Ishizuka O, Geshi N (2018) Geological Map of Hachiojima Volcano. Geological Map of Volcanoes, no. 20, Geological Survey of Japan, AIST, Tsukuba (in Japanese)
- Isshiki N (1958) Petrology of plutonic cognate ejecta from Nishi-yama volcano, Hachijo-jima, the seven Izu Islands, Japan. *Japanese J Geol Geograph* 29:55–74
- Isshiki N (1963) Petrology of Hachijo-jima Volcano Group, Seven Izu Islands, Japan. *J Fac Sci Univ Tokyo Sec 2*(15):91–134
- Isshiki N (1959) Geology of the Hachijo-jima. Geological Survey of Japan, AIST, Tsukuba (in Japanese with English abstract)
- Kaneoka I, Isshiki N, Zashu S (1970) K-Ar ages of the Izu-Bonin Islands. *Geochem J* 4:53–60
- Kawamoto T (1992) Dusty and honeycomb plagioclase: indicators of processes in the Uchino stratified magma chamber, Izu Peninsula, Japan. *J Volcanol Geotherm Res* 49:191–208
- Kimata F, Irwan M, Fukano K (2004) Ground deformation at Hachijo Island, Japan on 13–22 August 2002 observed by GPS measurements and estimated dike intrusion model. *Bull Volcanol Soc Jpn* 49:13–22 (in Japanese with English abstract)
- Kita S, Okada T, Hasegawa A, Nakajima J, Matsuzawa T (2010) Existence of inter-plane earthquakes and neutral stress boundary between the upper and lower planes of the double seismic zone beneath Tohoku and Hokkaido, northeastern Japan. *Tectonophysics* 496:68–82
- Kuritani T (1999) Phenocryst crystallization during ascent of alkali basalt magma at Rishiri Volcano, northern Japan. *J Volcanol Geotherm Res* 88:77–97
- Kuritani T, Nakamura E (2002) Precise isotope analysis of nanogram-level Pb for natural rock samples without use of double spikes. *Chem Geol* 186:31–43
- Kuritani T, Nakamura E (2003) Highly precise and accurate isotopic analysis of small amounts of Pb using  $^{205}\text{Pb}$ - $^{204}\text{Pb}$  and  $^{207}\text{Pb}$ - $^{204}\text{Pb}$ , two double spikes. *J Anal Atom Spectrom* 18:1464–1470
- Kuritani T, Shimizu K, Ushikubo T, Xia Q-K, Liu J, Nakagawa M, Taniuchi H, Sato H, Doi N (2021a) Tracing the subducting Pacific slab to the mantle transition zone with hydrogen isotopes. *Sci Rep* 11:18755
- Kuritani T, Sato E, Wada K, Matsumoto A, Nakagawa M, Zhao D, Shimizu K, Ushikubo T (2021b) Condition of magma generation at the Me-akan volcano, northern Japan. *J Volcanol Geotherm Res* 417:107323
- Liu X, Zhao D (2016) Backarc spreading and mantle wedge flow beneath the Japan Sea: insight from Rayleigh-wave anisotropic tomography. *Geophys J Int* 207:357–373
- Nakamura M, Shimakita S (1998) Dissolution origin and syn-entrapment compositional change of melt inclusion in plagioclase. *Earth Planet Sci Lett* 161:119–133
- Nakano S, Yamamoto T, Isshiki N (1991) Major-element chemistry of Nishiyama volcano, Hachiojima. *J Mineral Petrol Econom Geol* 86:72–81 (in Japanese with English abstract)
- Nakano S, Yamamoto T, Isshiki N (1997) Chemical compositions of the Hachijo-jima volcano group, Izu islands: comparison between the Higashiyama and Nishiyama volcanoes based on chemical analyses of surficial samples. *Bull Geol Survey Jpn* 48:93–105 (in Japanese with English abstract)
- Newman S, Lowenstern JB (2002) VOLATILECALC: a silicate melt-H<sub>2</sub>O-CO<sub>2</sub> solution model written in Visual Basic for excel. *Comput Geosci* 28:597–604
- Noguchi T, Shinjo R, Ito M, Takada J, Oomori T (2011) Barite geochemistry from hydrothermal chimneys of the Okinawa Trough: insight into chimney formation and fluid/sediment interaction. *J Mineral Petrol Sci* 106:26–35
- Pin C, Zaldugui JFS (1997) Sequential separation of light rare-earth elements, thorium and uranium by miniaturized extraction chromatography:

- application to isotopic analyses of silicate rocks. *Anal Chim Acta* 339:79–89
- Pin C, Briot D, Bassin C, Poitrasson F (1994) Concomitant separation of strontium and samarium-neodymium for isotopic analysis in silicate samples, based on specific extraction chromatography. *Anal Chim Acta* 298:209–217
- Putirka KD (2008) Thermometers and barometers for volcanic systems. *Rev Mineral Geochem* 69:61–120
- Suga K (1993) The latest activities of Higashiyama Volcano and development of Nishiyama Volcano, Hachijojima during past 10000 years. *Bull Volcanol Soc Jpn* 38:115–127 **(in Japanese with English abstract)**
- Suga K (1994) Volcanic history of Higashiyama, Hachijojima. *Bull Volcanol Soc Jpn* 39:13–24 **(in Japanese with English abstract)**
- Suga K (1998) The evolution process and its characteristics in the Hachijojima volcanic group, Izu-Bonin arc. *Quaternary Res* 37:59–75 **(in Japanese with English abstract)**
- Sugihara S (1998) Tephrochronological study of Higashiyama volcano at Hachijojima, Izu islands. *J Geograph* 107:390–420
- Sun SS, McDonough WF (1989) Chemical and isotopic systematics of oceanic basalts: implications for mantle composition and processes Magmatism in the Ocean Basins. *Geol Soc London Spec Pub* 42:313–345
- Tamura Y, Ishizuka O, Stern RJ, Nichols ARL, Kawabata H, Hirahara Y, Chang Q, Miyazaki T, Kimura J-I, Embley RW, Tatsumi Y (2014) Mission immiscible: distinct subduction components generate two primary magmas at Pagan Volcano, Mariana arc. *J Petrol* 55:63–101
- Taniuchi H, Kuritani T, Nakagawa M (2021) Na/K diversity of primary basaltic magmas induced by the separation of slab-derived supercritical liquid: Implications from alkali basaltic lavas from Rishiri Volcano, southern Kuril Arc. *J Petrol* 62:1–22
- Tsuchiyama A (1985) Dissolution kinetics of plagioclase in the melt of the system diopside–albite–anorthite, and origin of dusty plagioclase in andesites. *Contrib Mineral Petrol* 89:1–16
- Tsukui M, Hoshino K (2002) Magmatic differentiation of Hachijo-Nishiyama volcano, Izu islands, Japan. *Bull Volcanol Soc Jpn* 47:57–72 **(in Japanese with English abstract)**
- Tsukui M, Moriizumi M, Suzuki M (1991) Eruptive history of the Higashiyama Volcano, Hachijo Island during the last 22,000 years. *Bull Volcanol Soc Jpn* 36:345–356 **(in Japanese with English abstract)**
- Yokoyama T, Nagai Y, Hinohara Y, Mori T (2017) Investigating the influence of non-spectral matrix effects in the determination of twenty-two trace elements in rock samples by ICP-QMS. *Geostand Geoanal Res* 41:221–242

## Publisher's Note

Springer Nature remains neutral with regard to jurisdictional claims in published maps and institutional affiliations.

Submit your manuscript to a SpringerOpen<sup>®</sup> journal and benefit from:

- Convenient online submission
- Rigorous peer review
- Open access: articles freely available online
- High visibility within the field
- Retaining the copyright to your article

---

Submit your next manuscript at ► [springeropen.com](https://www.springeropen.com)

---